Moments-Based Reduced Spectral Wave Modeling of Frequency-and-Directional Spreading Effects on Wave-Induced Longshore Currents

Yang Zhang[1] and Andrew B. Kennedy[2]

Abstract: Often, nearshore radiation stresses are approximated using the monochromatic wave assumption, although this can have significant errors when the incident waves have finite frequency and/or directional spread. Consequently, the resulting wave-driven currents could be predicted erroneously or, when fitting to observations, biased model parameters such as the bottom friction coefficient may result. We develop and test a moments-based reduced spectral wave model which includes the leading order effects of wave frequency and directional spreading. This model solves the evolution equations of wave moments, which are integrations of the wave action balance equation multiplied by weighting functions over frequencies and directions. An assumption of analytical Gaussian distribution for the frequency-direction spectrum is made to develop a simple five-parameter system that contains information on the wave height, period, direction, frequency bandwidth, and directional bandwidth. Using this model, we investigate the finite bandwidth effects on the wave field and radiation stresses. The directional spreading is found to have a strong impact on the radiation stress, with a larger directional bandwidth resulting in smaller radiation stresses. However, the frequency spreading has much less impact. The spectral wave breaking based on the roller concept is considered in this wave model. After coupling with a circulation model based on the shallow water equations, simulation results compare favorably with the DUCK94 field data for waves and longshore currents but show strong dependence on the directional bandwidth.

DOI: 10.1061/(ASCE)WW.1943-5460.0000044

CE Database subject headings: Littoral currents; Wave spectra; Stress.

Author keywords: Moments-based spectral wave model; Frequency spreading; Directional spreading; Longshore currents.

Introduction

Waves begin to feel the sea bottom as they propagate into shallow nearshore areas and various wave transformations take place including wave shoaling, refraction, diffraction, and breaking. Since wave momentum fluxes are proportional to the wave energy, changes in the wave field will lead to changes in the momentum fluxes and generate wave-induced nearshore currents. Alongshore currents in particular are commonly generated by obliquely incident waves breaking on a beach. The important role of alongshore currents in coastal processes has long been recognized and their measurement and prediction have received much attention from scientists and coastal engineers (Bowen 1969; Longuet-Higgins 1970; Thornton 1970; Guza et al. 1986; among many others).

Longshore Currents

The development of the radiation stress concept by Longuet-Higgins and Stewart (1964) has made it possible to simulate wave-induced currents using mathematical models. In past decades, a variety of current models have been developed and used to study wave-induced currents in coastal areas. Early one-dimensional models were simultaneously developed by Longuet-Higgins (1970), Bowen (1969), and Thornton (1970). Thornton and Guza (1986) developed a model that took into account irregular wave breaking and successfully reproduced the measured alongshore current profile on a planar beach. For alongshore uniform barred beaches, models (e.g., Church and Thornton 1993; Feddersen et al. 1998) predicted longshore current profiles with maxima not over the bar crests, which are not consistent with laboratory experiments and field observations. This failure may result from the neglect of rollers in the wave forcing (e.g., Lippmann et al. 1996; Reniers and Battjes 1997; Ruessink et al. 2001). The surface wave rollers give a correction to the wave radiation stresses and consequently alter the wave forcing in the surf zone. Ruessink et al. (2001) demonstrated that including the rollers in the wave forcing greatly improved the predictions of the observed wave-induced longshore currents over barred beaches.

Spectral Wave Models

When modeling wave-induced currents it is often assumed that the wave spectrum is narrowbanded resulting in a single representative direction and frequency to approximate the irregular waves (e.g., Church and Thornton 1993; Özkan-Haller and Kirby 1999; Ruessink et al. 2001). However, in situations where the

[1]Halcrow, 22 Cortlandt St., 31st Floor, New York, NY 10007 (corresponding author). E-mail: Zhangy@halcrow.com

[2]Dept. of Civil Engineering and Geological Sciences, Univ. of Notre Dame, Notre Dame, IN 46556. E-mail: Andrew.kennedy@nd.edu

Note. This manuscript was submitted on May 22, 2009; approved on December 2, 2009; published online on February 4, 2010. Discussion period open until December 1, 2010; separate discussions must be submitted for individual papers. This paper is part of the ***Journal of Waterway, Port, Coastal, and Ocean Engineering***, Vol. 136, No. 4, July 1, 2010. ©ASCE, ISSN 0733-950X/2010/4-200–214/$25.00.

wave spectrum is not narrowbanded, the resulting wave field may differ substantially between irregular, multidirectional waves and the monochromatic approximation (e.g., Vincent and Briggs 1989; Panchang et al. 1990). In addition, the monochromatic approximation can cause significant errors in estimating the wave radiation stresses, even though the wave heights may be similar. Battjes (1972) first investigated the effect of frequency-and-directional spreading on the radiation stresses and derived mathematical expressions for corrections to the monochromatic approximations according to the linear wave theory. Feddersen (2004) compared the monochromatic-approximated radiation stresses to the true radiation stresses calculated using a moment-based technique (Elgar et al. 1994) in 8-m water depth during DUCK94 and SandyDuck field experiments and found that the component S_{xy} was overestimated systematically by up to 60% by the monochromatic approximation. Using parameterized wave spectra, Feddersen found that the difference between the approximated and true radiation stresses is mainly due to the directional spread, whereas the frequency spread only has a minor effect.

Locally generated waves usually have a broad frequency-directional spectrum. In deep water, the one-sided directional bandwidth of the wave spectrum is typically 30° (Holthuijsen 2007). Additionally, a distantly generated ocean swell often arrives at beaches with finite frequency and directional spread. The inclusion of these frequency-and-directional spreading effects can be accomplished in several ways. One approach is to use phase-resolving monochromatic wave models to go through every individual wave component and calculate the wave statistics afterward such as a model based on the mild-slope equation (e.g., Panchang et al. 1990; Chawla et al. 1998) or to use a model based on the Boussinesq equations, in which all components are calculated simultaneously (e.g., Chen et al. 2003). However, these models tend to be quite expensive. Alternatively, full spectral models such as WAM (WAMDI Group 1988), WAVEWATCH III (Tolman 1991), or SWAN (Booij et al. 1999) are common. These models solve the full evolution of wave spectra in both engineering practice and research. However, the wave spectrum needs to be solved not only in spatial dimensions and time but also in frequency and directional space. Therefore, these models are usually computationally expensive.

Study Objectives

At present, there is no method intermediate between a full spectral model and the quasimonochromatic approximation. To fill this gap, we introduce here a reduced spectral, moments-based wave model by integrating the weighted governing equations over all frequencies and directions of the spectral evolution. The model thus solves for wave moments, which can contain information on other important wave parameters in addition to the RMS wave height, mean frequency, and mean wave angle provided by monochromatic-based models. The model developed here contains additional information on the frequency bandwidth and directional bandwidth. Thus the moments-based model, when coupled with a circulation model as the wave driver, enables the direct investigation of frequency-and-directional spreading effects on the resulting wave-induced currents. Unlike full spectral models, moments-based models do not need to be solved in the full spectral domain for all frequencies and directions. Instead, several equations of wave moments will be solved only in space and time (for unsteady problems). Therefore, a moments-based wave model will require much less computational effort than standard spectral models although more than monochromatic models. It should, however, be emphasized that this moments-based model is still spectrally averaged, so it will not include effects from fluctuating wave groups as would a complete phase-resolving model (e.g., Chen et al. 2003). The reduced model is expected to be most useful in coastal areas, where it might be used for simulations of wave transformation that would be costly to perform using a full spectral model.

In this study, we use the moments-based model to examine the effects of frequency-and-directional spreading on wave-induced longshore currents by coupling the wave model with a two-dimensional (2D) circulation model based on the nonlinear shallow water equations. The new wave model is described in detail in the following section including the derivation of governing equations, solution methods, and model tests. Using the coupled wave/circulation model, we simulate the wave-induced longshore currents over a barred beach at Duck, N.C. during a storm event and the model results are compared against the field data. A roller model including the effect of the directional spreading is developed and corrections due to surface wave rollers are taken into account in simulations. Sensitivity tests on the impact of frequency and directional bandwidths upon the resulting longshore currents are conducted. We also investigate the apparent variation of the bottom friction coefficient in longshore flows with changing directional bandwidth.

Moments-Based Wave Model

Derivation of Governing Equations

The wave spectrum is defined as the Fourier transform of covariance of the sea surface, providing a statistical description of the complex sea states. The physical meaning of the wave frequency-direction spectrum is that it specifies the distribution of the wave energy over all frequencies and directions. When the random sea elevation is treated as a stationary Gaussian process, the statistical characteristics of a frequency spectrum can be expressed in terms of the spectral moments of the frequency spectrum $F(\sigma)$ (Holthuijsen 2007)

$$m_n = \int_0^{+\infty} \sigma^n F(\sigma) d\sigma, \quad n = 0,1,2,\ldots \tag{1}$$

where σ=intrinsic angular frequency (Willebrand 1975). These will converge for exponents, n, that are not too large. Extending and generalizing this concept, the general wave moment $E_n(\mathbf{x},t)$ of a frequency-directional spectrum $F(\mathbf{x},t;\sigma,\theta)$ could be defined by

$$E_n(\mathbf{x},t) = \int_0^{+\infty} \int_{-\pi}^{\pi} w_n(\sigma,\theta) F(\mathbf{x},t;\sigma,\theta) d\sigma d\theta \tag{2}$$

where θ=wave angle; $w_n(\sigma,\theta)$ are as yet undefined weighting functions; and the subscript n=index of the weighting function and moment. Because the wave spectra are generally clustered around certain frequencies and directions, it seems plausible to suggest that, with intelligent choices of weighting functions, only a relatively small number of moments might be needed to represent the wave spectra that are not too complex.

In contrast, full spectral wave models (e.g., SWAN and WAVEWATCH III) represent the wave spectrum for a discrete number of frequencies and directions at each location in space.

Although numbers vary, a typical implementation might use 25 frequencies and 24–36 directions, giving 600–900 degrees of freedom at each grid location. The many spectral components can lead to large memory requirements and slow execution times as they solve the spectral wave action balance for these frequencies and directions. The fundamental equation of spectral evolution can be written as (Hasselmann et al. 1973)

$$\frac{\partial}{\partial t}\left(\frac{F}{\sigma}\right)+\nabla\cdot\left[(\mathbf{c_g}+\mathbf{U})\frac{F}{\sigma}\right]+\frac{\partial}{\partial\sigma}\left(c_\sigma\frac{F}{\sigma}\right)+\frac{\partial}{\partial\theta}\left(c_\theta\frac{F}{\sigma}\right)=\frac{S_{\mathrm{tot}}}{\sigma} \quad (3)$$

where $\mathbf{c_g}$ and $\mathbf{U}$=group velocity vector and ambient current vector, respectively. c_σ and c_θ=propagation velocities in spectral spaces (frequency and direction space). ∇=2D gradient operator and $S_{\mathrm{tot}}(\mathbf{x},t;\sigma,\theta)$ represents the effects of wave generation, dissipation, and nonlinear energy transfers.

With the definition of wave moments, evolution equations for these moments can be obtained by multiplying the standard wave action balance Eq. (3) by the weighting functions $w_n(\sigma,\theta)$ and then integrating over all frequencies and directions. These moments are only functions of time at a given location in geographical space, so if there are N total moments then there will only be N evolution equations at each point in space and time and consequently the computational efforts can be greatly reduced. The key question then becomes how to choose a proper weighting function. The weighting functions should be easy to treat mathematically and more important should result in wave moments that make it simple to evaluate the wave properties of most interest (e.g., RMS wave height; mean direction; peak frequency; and the frequency and directional bandwidths). In this study, the moments are defined using the weighting function $\sigma^n e^{im\theta}$. The corresponding frequency moments are consistent with the traditional definition and the directional moments are similar with the definition of Kuik et al. (1988). Following Eq. (2), the wave moment $E_{n,m}$ is written as

$$E_{n,m}(\mathbf{x},t)=\int_0^{+\infty}\int_{-\pi}^{\pi}\sigma^n e^{im\theta}F(\mathbf{x},t;\sigma,\theta)d\sigma d\theta \quad (4)$$

where $n,m=0,1,2,\ldots$=indices of moments. If $m=0$, $E_{n,m}$=nth frequency moment of the wave spectra. If $n=0$, $E_{n,m}$ becomes the mth directional moment. It reduces to the wave variance $E_{0,0}=H_{\mathrm{RMS}}^2/8$ when both m and n are equal to zero. This is not the only possible choice of weighting functions; it works well for small exponents, n, but will not converge when $n\geqslant 4$. Thus, if large numbers of weighting functions are desired, other weights will prove more useful. However, here we only use relatively small exponents so convergence is not an issue.

After multiplying Eq. (3) by $\sigma^{n+1}e^{im\theta}$, using the product rule for derivatives, and integrating over all frequencies and directions, we arrive at

$$\begin{aligned}&\frac{\partial}{\partial t}E_{n,m}+\nabla\cdot\int_0^{+\infty}\int_{-\pi}^{\pi}(\mathbf{c_g}+\mathbf{U})\sigma^n e^{im\theta}Fd\sigma d\theta\\&+\int_0^{+\infty}\int_{-\pi}^{\pi}\frac{\partial}{\partial\sigma}(c_\sigma\sigma^n e^{im\theta}F)d\sigma d\theta\\&+\int_0^{+\infty}\int_{-\pi}^{\pi}\frac{\partial}{\partial\theta}(c_\theta\sigma^n e^{im\theta}F)d\sigma d\theta\\&-(n+1)\int_0^{+\infty}\int_{-\pi}^{\pi}c_\sigma\sigma^{n-1}e^{im\theta}Fd\sigma d\theta\\&-im\int_0^{+\infty}\int_{-\pi}^{\pi}c_\theta\sigma^n e^{im\theta}Fd\sigma d\theta=\int_0^{+\infty}\int_{-\pi}^{\pi}S_{\mathrm{tot}}\sigma^n e^{im\theta}d\sigma d\theta\end{aligned} \quad (5)$$

Physically, since $\sigma^n F(\sigma=0)=0$ and $\sigma^n F(\sigma=\infty)=0$ (for sufficiently small n), and because $e^{im\pi}=e^{-im\pi}$ with integer m, it is obvious that

$$\int_0^{+\infty}\int_{-\pi}^{\pi}\frac{\partial}{\partial\sigma}(c_\sigma\sigma^n e^{im\theta}F)d\sigma d\theta=0 \quad (6a)$$

$$\int_0^{+\infty}\int_{-\pi}^{\pi}\frac{\partial}{\partial\theta}(c_\theta\sigma^n e^{im\theta}F)d\sigma d\theta=0 \quad (6b)$$

Eq. (5) is then reduced to

$$\begin{aligned}&\frac{\partial}{\partial t}E_{n,m}+\nabla\cdot\int_0^{+\infty}\int_{-\pi}^{\pi}(\mathbf{c_g}+\mathbf{U})\sigma^n e^{im\theta}Fd\sigma d\theta\\&-(n+1)\int_0^{+\infty}\int_{-\pi}^{\pi}c_\sigma\sigma^{n-1}e^{im\theta}Fd\sigma d\theta\\&-im\int_0^{+\infty}\int_{-\pi}^{\pi}c_\theta\sigma^n e^{im\theta}Fd\sigma d\theta=\int_0^{+\infty}\int_{-\pi}^{\pi}S_{\mathrm{tot}}\sigma^n e^{im\theta}d\sigma d\theta\end{aligned} \quad (7)$$

Note that the wave spectrum $F(\mathbf{x},t;\sigma,\theta)$ is still in the above equation. In a moments-based reduced model, the moments, $E_{n,m}$, are the only known quantities and will not uniquely define the detailed variation of the wave spectrum $F(\mathbf{x},t;\sigma,\theta)$. This introduces a closure problem much like those found in computations of the turbulent flow, where integrals involving the full wave spectrum need to be expressed in terms of moment $E_{n,m}$ and/or moments of other orders. To uniquely define all terms in the governing equations in terms of wave moments, several approximations and assumptions were made.

The first assumption deals with the shape of the spectrum, which is not uniquely defined by a finite number of moments. For this first investigation of a reduced system, a 5-degree-of-freedom system was used which provided information on the wave height, peak frequency, peak direction, and both frequency and directional bandwidths. The system was assumed to be separable in frequency and direction, so that $F(\sigma,\theta)=E_{0,0}M(\sigma)D(\theta)$. Because $E_{0,0}$ is the definition of the wave variance, it follows that the frequency and directional distributions, $M(\sigma)$ and $D(\theta)$, are probability density functions and integrate to unity over the frequency and direction, respectively.

For the frequency spectrum $M(\sigma)$, it would be possible to use standard spectral shapes such as JONSWAP (Joint North Sea Wave Project) or Pierson-Moskowitz (PM); evaluate all integrals numerically; and compose a lookup table. However, it is unclear how these spectra would be modified to account for varying spectral bandwidths (e.g., narrowbanded swell versus broadbanded sea). Thus we have chosen to use an analytical Gaussian distribution in frequency, where changing bandwidth is trivial. The integrals in Eq. (7) were evaluated by expanding the velocities $\mathbf{c_g}$, $\mathbf{c}_\sigma$, and $\mathbf{c}_\theta$ using Taylor series approximations, which were then integrated analytically. Another approach would be to integrate the equations numerically but, as will be seen, there is little difference between the two approaches in terms of accuracy. Because the Gaussian assumption theoretically gives small positive values for negative frequencies this closure should not be used for strongly broadbanded seas.

A Gaussian assumption is also used for the directional distribution. Other possibilities include cosine power functions, which are commonly used in defining boundary conditions in spectral wave models (Holthuijsen 1983). However, there do not appear to be any obvious advantages to cosine distributions, while integrals of the Gaussian functions can be integrated analytically using standard relations and have clearly visible relations to the directional bandwidth.

With these assumptions, the parameterized frequency-directional spectrum used for closing the reduced system then becomes

$$F(x,y,t;\sigma,\theta) = E_{0,0}\frac{1}{\sqrt{2\pi}S_\sigma}\exp\left[-\frac{1}{2}\left(\frac{\sigma-\sigma_m}{S_\sigma}\right)^2\right]\frac{1}{\sqrt{2\pi}S_\theta}\times\exp\left[-\frac{1}{2}\left(\frac{\theta-\theta_m}{S_\theta}\right)^2\right] \quad (8)$$

where σ_m=mean intrinsic frequency; S_σ=one-sided frequency bandwidth with units of rad/s; θ_m=mean direction; and S_θ=one-sided directional bandwidth. This closure is suitable for modeling waves with a single-peaked spectrum in both frequency and direction. It is not suitable for modeling, for example, combinations of local wind waves and distant swell. A system composed of multiple spectra of this type might be used in this case, but will not be treated here.

With the Gaussian spectral closure given in Eq. (8), the general moment $E_{n,m}$ can be written as

$$E_{n,m} = \frac{E_{0,0}}{\sqrt{2\pi}}e^{-m^2S_\theta^2/2}e^{im\theta_m}\begin{cases}\displaystyle\sum_{k=0}^{n}\frac{n!}{k!(n-k)!}S_\sigma^{n-k+1}\sigma_m^k 2^{(n-k+1)/2}\Gamma[(n-k+1)/2], & n-k=0,2,4,\ldots\\ 0, & \text{otherwise}\end{cases} \quad (9)$$

where $\Gamma[(n-k+1)/2]$=gamma function. Detailed derivations are given in the section "Derivation of Wave Moments." Evaluating the integrals in Eq. (7) in terms of moments is straightforward but lengthy (see the section "Evaluation of the Integrals in Wave Governing Equations" for details). Generally, for moment $E_{n,m}$, the evolution equation has the following form:

$$\frac{\partial}{\partial t}E_{n,m} + I1 + I2 + I3 = 0 \quad (10)$$

where integrals $I1$, $I2$, and $I3$=functions of $(E_{n,m}, E_{n+i,m+j}, \sigma_m, \theta_m, S_\sigma, S_\theta)$, as given in Appendix I, "Evaluation of the Integrals in Wave Governing Equations." $E_{n+i,m+j}$ ($i=1,2$ and $j=-2,-1,1,2$) are moments of other orders rather than $E_{n,m}$. The relations between moments are defined by Eq. (9). The governing equations in explicit form for the single frequency, directional waves without ambient currents are given in Appendix I, "Explicit Equations for Regular Directional Waves."

Theoretically, the moments of the wave spectrum can be taken to any order as necessary. However, the values of higher-order moments are rather sensitive to noise in the high-frequency range of the spectrum (Holthuijsen 2007) and problems with convergence will be encountered for large exponents n. Generally, more information can be obtained from more moments. At the same time, however, more moments involved lead to a more complicated system. So in practice, the number of moments used should be determined by the specific wave spectrum and by the accuracy requirement of problem interested. In this study, a system with five equations solving the five moments, $E_{0,0}, E_{1,0}, E_{2,0}, (E_{0,1})_R$, and $(E_{0,1})_I$, is developed. The specific expressions of these five equations can be easily obtained with the equation of the general moment $E_{n,m}$ derived in the "Evaluation of the Integrals in Wave Governing Equations" and will not be reproduced here for brevity. This five-parameter system is relatively simple but contains information on the following: the RMS wave height, mean period, mean direction, frequency bandwidth, and directional bandwidth. The system itself can be used as an alternative for the full spectral wave models to some degree, especially when well-defined wave spectra are involved such as narrowbanded Gaussian-type spectra. What is even more important is that this system can serve as a foundation for a more comprehensive model that is able to simulate the realistic wave spectra accurately.

Model Tests

For a first test, the results from the moments-based wave model are compared to the analytical solutions for the transformation of irregular waves on a planar beach. The bathymetry consists of a flat bottom with 10-m depth followed by a constant slope of 1:50 as shown in Fig. 1. For testing purposes, no energy dissipation is assumed.

Without dissipation and with no ambient currents, the wave energy conservation equation for stationary, monochromatic incident waves can be written as

$$Ec_g\cos\theta = (Ec_g\cos\theta)_0 \quad (11)$$

where the subscript "0" stands for incident wave conditions; and E=total wave energy. This equation can easily be solved analytically according to Snell's law. For spectral waves, the analytical solutions are not as apparent but still can be obtained by splitting the total wave spectrum into monochromatic components, with each component corresponding to a direction and a frequency. Eq. (11) is then solved for all components and wave moments can then be obtained following their definition. This will become used for computing numerically exact spectral wave transformation over cross-shore varying topography for comparison with the approximate moments-based model.

Numerically, the governing equations of the moments-based model are solved in time given the initial condition and the offshore boundary condition. A second-order Runge-Kutta method

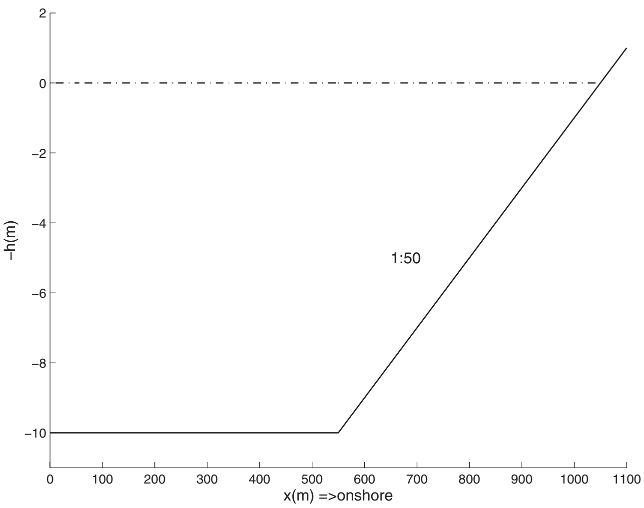

Fig. 1. Planar beach bathymetry with a slope of 1:50 connecting to a flat bed with 10-m water depth. Water depth is 1 m at $x=1{,}000$ m.

is used for temporal differencing and the third-order upwind scheme (also known as QUICK) is used for spatial derivatives. Stationary incident waves of $T_p=4$ s and $H_{\mathrm{RMS}}=1$ m at the offshore boundary are used for this test. The computational domain is $L_x=1{,}000$ m in the cross-shore direction. The spatial grid size used is $\Delta x=2$ m, with a time step of $\Delta t=0.2$ s. The total run time is 30 min, which is long enough for the wave field to reach a steady state.

In the first set of simulations, normally incident unidirectional waves (i.e., $S_\theta=0°$, $\theta_m=0$) but with finite frequency bandwidths are used to examine the model's performance in simulating the shoaling of irregular waves. As discussed previously, the present wave model uses a Gaussian closure. However, field measurements of the ocean wave spectrum have shown that the one-dimensional frequency spectrum appears to roughly have a universal shape: the JONSWAP spectrum (Hasselmann et al. 1973). Therefore, it is necessary to examine the differences between using JONSWAP spectra and using Gaussian spectra as an approximation. Fig. 2(a) shows the comparison of the JONSWAP wave frequency spectrum and a Gaussian-shaped spectrum with the same peak frequency 0.25 Hz; the same frequency bandwidth of $S_\sigma/\sigma_m=0.11$; and the same RMS wave height of 1 m.

Fig. 2(b) shows comparisons between three shoaling spectra: numerically exact results from the shoaling of an initial JONSWAP spectrum; numerically exact results using the initially Gaussian-shaped spectrum of Fig. 2(a); and results from the moments-based model with the Gaussian closure. The maximum height differences between the exact and moments-based transformation of the initially Gaussian spectrum are around 1% suggesting that the moments-based model approximates the transformation well. Differences in transformation between the Gaussian and JONSWAP spectra are still small, with a maximum difference of 3.6% in very shallow water (where waves would likely be breaking in any case) and a RMS difference of less than 1%. This suggests that using a Gaussian spectrum to approximate a more realistic JONSWAP in this simple case will not introduce large errors.

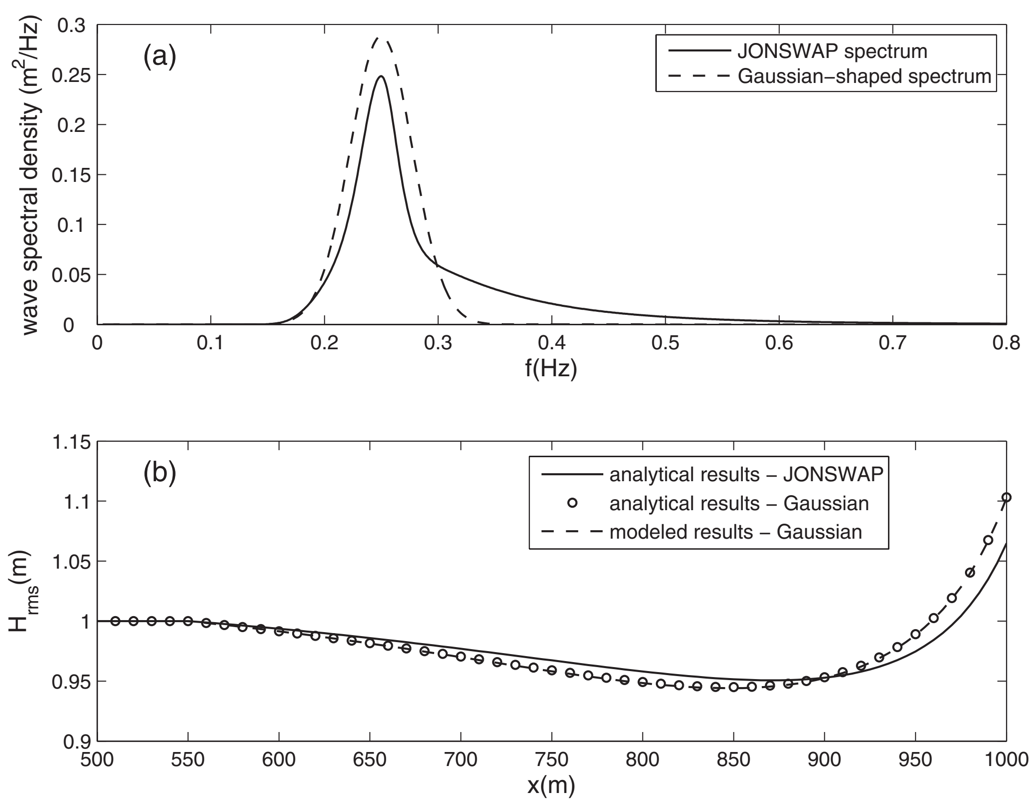

Fig. 2. (a) JONSWAP wave frequency spectrum and its approximation using the Gaussian-shaped spectrum with the same peak frequency 0.25 Hz and the frequency bandwidth $S_\sigma/\sigma_m=0.11$, and the same RMS wave height of 1 m. (b) Comparison of analytical results for inviscid shoaling for the initially JONSWAP spectrum (solid); analytical shoaling of the initially Gaussian-shaped spectrum (circles); and the five-parameter reduced model results with the Gaussian closure.

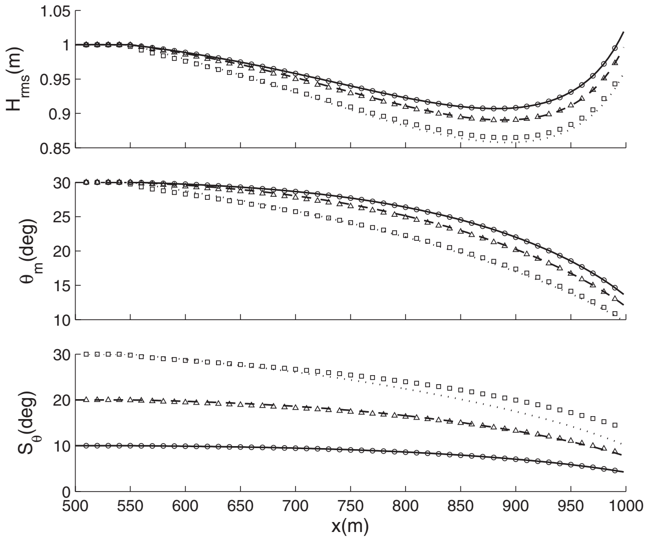

Fig. 3. Transformation of multidirectional waves over the sloping beach of Fig. 1: (a) H_{RMS}; (b) mean direction θ_m; and (c) directional bandwidth S_θ. A Gaussian incident spectrum is used with $\sigma_m = 2\pi/4$, $S_\sigma = 0$, and $\theta_m = 30°$. Symbols (circle, diamond, and square) indicate analytical shoaling of the original spectrum using $S_\theta = 10°, 20°, 30°$, respectively. Lines represent the results from the five-parameter model. Nonbreaking waves are assumed.

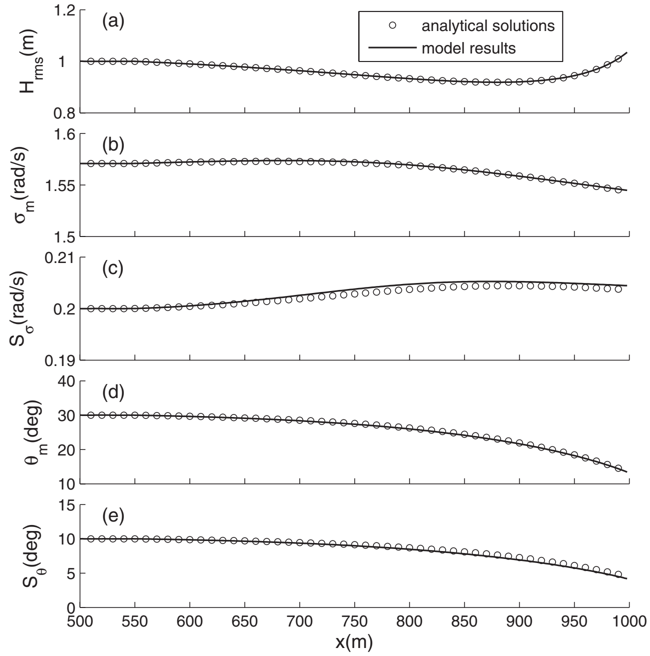

Fig. 4. Comparison of five-parameter model results (lines) with analytical solutions (circles) for incident Gaussian spectra: $\theta_m = 30°$, $S_\sigma = 0.2$ rad/s, and $S_\theta = 10°$. (a) H_{RMS}; (b) mean frequency σ_m; (c) frequency bandwidth S_σ; (d) mean direction θ_m; and (e) directional bandwidth. Nonbreaking waves are assumed.

In the second set of simulations, waves are used with a single frequency, i.e., $S_\sigma = 0$, and with mean incident angle $\theta_m = 30°$, but finite directional bandwidth. Fig. 3 shows a comparison of the moments-based model results with the analytical solutions for directional bandwidths $S_\theta = 10°, 20°, 30°$. We observe that the model results are in good agreement with the analytical solutions. For smaller directional bandwidth $S_\theta = 10°$ and $S_\theta = 20°$, the cross-shore variations of H_{RMS}, θ_m, and S_θ are accurately predicted. For the case $S_\theta = 30°$, H_{RMS} is predicted with a minor discrepancy from the analytical results, and S_θ is underpredicted with maximum error close to the shore. It is also evident that the shoaling wave heights are smaller for a broader wave directional spectrum and the bandwidth S_θ decreases as waves approach the shoreline. This directional narrowing is expected and consistent with Snell's law for bathymetric refraction: waves tend to travel in the direction normal to bottom contours; thus, all wave components bend to the shore-normal direction and consequently both the mean direction and the directional bandwidth decrease as waves travel toward the shore.

Simulations for incident waves with both nonzero frequency bandwidths and directional bandwidths are also conducted. Fig. 4 shows model results of waves with $S_\sigma = 0.2$ rad/s ($S_\sigma/\sigma_m \approx 0.127$) and $S_\theta = 10°$ compared to a numerically exact transformation with the same original spectrum. The cross-shore variations of H_{RMS}, σ_m, and θ_m are accurately predicted, and only a slight overestimation in S_σ and underestimation in S_θ are observed. Overall, this test demonstrates the capability of the present model to predict the shoaling and refraction of irregular waves with finite frequency and directional bandwidth.

Radiation Stresses

Because wave radiation stress gradients define forcing, an accurate estimate of radiation stresses is critical in modeling wave-induced currents. For simplicity, radiation stresses computed using basic wave statistics (H_{RMS}, peak frequency, and mean direction) have been used for many years to drive nearshore circulation models (e.g., Church and Thornton 1993; Ruessink et al. 2001). For random waves, however, the wave radiation stress is a function of the frequency-direction spectrum and the monochromatic approximation can result in significant errors (e.g., Battjes 1972; Feddersen 2004).

The present wave model solves the frequency bandwidth and directional bandwidth in addition to the wave height, mean direction, and mean frequency. Therefore, it can provide a more accurate estimate of the radiation stress by including the frequency-and-directional spreading. For a monochromatic wave of height H, the radiation stress can be written as (Longuet-Higgins and Stewart 1964)

$$S_{ij} = E[n(k_i k_j/k^2 + \delta_{ij}) - \delta_{ij}/2] \tag{12}$$

where $E = 1/8\rho g H^2$ and $n = c_g/c$. For random waves, according to the linear wave theory the radiation stress is written as (Battjes 1972)

$$S_{ij} = \rho g \int_0^{+\infty} \int_{-\pi}^{\pi} \left[\frac{c_g(\sigma)}{c(\sigma)} (k_i k_j/k^2 + \delta_{ij}) - \delta_{ij}/2 \right] F(\sigma,\theta) d\sigma d\theta \tag{13}$$

Assuming $F(\sigma,\theta)$ is separable as $F(\sigma,\theta) = M(\sigma)D(\theta)$, where $M(\sigma)$ = function of frequency distribution, and $\int_0^\infty M(\sigma) d\sigma = E_{0,0} = H_{\text{RMS}}^2/8$, and $D(\theta)$ = directional distribution and normalized so that $\int_{-\pi}^{\pi} D(\theta) d\theta = 1$. With these used in Eq. (13), we obtain

$$S_{xx} = \rho g \int_0^{+\infty} \frac{c_g(\sigma)}{c(\sigma)} M(\sigma) d\sigma \left[1 + \int_{-\pi}^{\pi} D(\theta) \cos^2 \theta d\theta \right] - \frac{1}{2} \rho g E_{0,0} \tag{14a}$$

$$S_{xy} = \rho g \int_0^{+\infty} \frac{c_g(\sigma)}{c(\sigma)} M(\sigma) d\sigma \int_{-\pi}^{\pi} D(\theta) \sin\theta \cos\theta d\theta \quad (14b)$$

$$S_{yy} = \rho g \int_0^{+\infty} \frac{c_g(\sigma)}{c(\sigma)} M(\sigma) d\sigma \left[1 + \int_{-\pi}^{\pi} D(\theta) \sin^2\theta d\theta \right] - \frac{1}{2}\rho g E_{0,0} \quad (14c)$$

To examine the effect of frequency spreading, unidirectional waves are assumed, with $D(\theta)=\delta(\theta-\theta_m)$, which is the delta function, Eq. (14b) reduces to

$$S_{xy} = \rho g \sin\theta_m \cos\theta_m \int_0^{+\infty} \frac{c_g(\sigma)}{c(\sigma)} M(\sigma) d\sigma \quad (15)$$

For any given $M(\sigma)$ and water depths, the integral in the above equation can be computed numerically. The error introduced by neglecting the frequency spreading is measured by the ratio of S_{xy} to $(S_{xy})_{\mathrm{mono}}$, which represents the monochromatic approximation

$$\frac{S_{xy}}{(S_{xy})_{\mathrm{mono}}} = \frac{\int_0^{+\infty} c_g(\sigma) M(\sigma)/c(\sigma) d\sigma}{E_{0,0} c_g(\sigma_m)/c(\sigma_m)} \quad (16)$$

In examining the effect of directional spreading on the radiation stress, the assumption of $M(\sigma)=E_{0,0}\delta(\sigma-\sigma_m)$ is made. Again, taking the component S_{xy}, for instance, after some algebra, the ratio can be written as

$$S_{xy}/(S_{xy})_{\mathrm{mono}} = \exp(-2S_\theta^2) \quad (17)$$

The above equation is valid for any nonzero mean wave angle. The expressions for S_{xx} and S_{yy} can be obtained similarly and will not be reproduced here.

Two types of empirical frequency spectra are used to examine the effects of the frequency spread: Gaussian-shaped spectra and the PM spectra (Pierson and Moskowitz 1964). For the Gaussian spectra, ratios of the true and approximate radiation stresses for 6-s waves with a water depth of 6 m are computed. Fig. 5(a) shows that, as the frequency bandwidth increases, the ratios change only slightly from 1 and the differences are less than 5% with a broad spectrum of $S_\sigma/\sigma_m=0.5$.

Fig. 5(b) shows that although all radiation stress components are underestimated somewhat for the PM spectrum, with the discrepancies increasing for larger f_p (i.e., intermediate-deep water waves for the fixed water depth of 6 m), the errors are not large. Thus, the frequency spreading does not have strong influences on the radiation stresses, which is consistent with Feddersen (2004). Although a realistic frequency spectrum may be considerably different from a Gaussian distribution or the PM spectrum, this strongly suggests that finite frequency spread does not change the wave radiation stresses significantly and the monochromatic approximation in calculating radiation stresses could be reasonable for most cases.

In contrast, the ratios of the true radiation stresses to the unidirectional approximations show a very strong dependence on the wave directional bandwidth S_θ as seen in Fig. 5(c). S_{xx} and S_{xy} are overestimated consistently by using the monochromatic approximation as S_θ increases, while S_{yy} is underestimated. With a directional spread of $S_\theta=30°$ (a typical one-sided directional bandwidth; Holthuijsen 2007), the monochromatic approximations overestimate S_{xy} by 73%, which will, without question, change the wave forcing and the wave-induced longshore currents considerably.

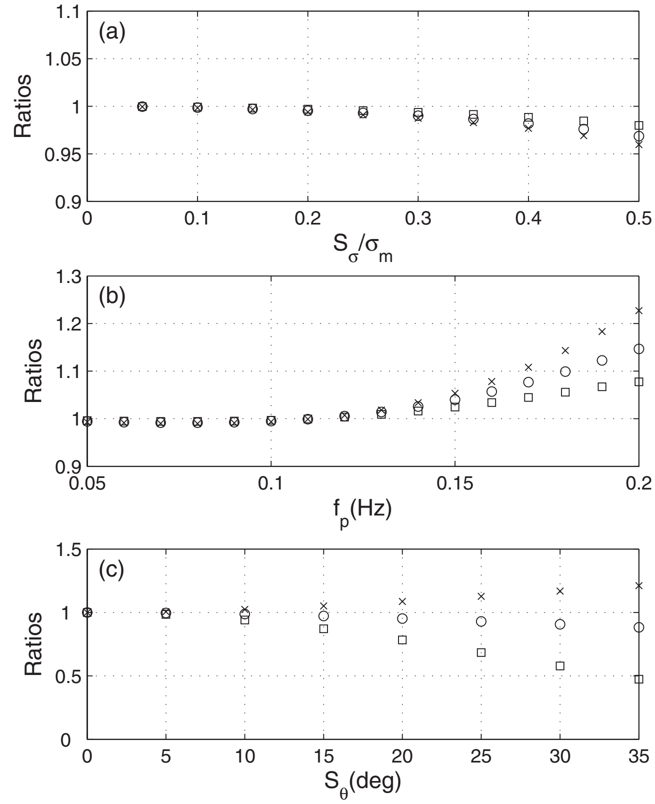

Fig. 5. Ratios of the true spectral radiation stress components to monochromatic radiation stresses with the same RMS wave height, mean direction, and peak frequency. (a) Gaussian spectra with varying frequency bandwidths, $\sigma_m=2\pi/6$, $\theta=30°$, $S_\theta=0$, and water depth $h=6$ m are used. (b) For PM spectra with varying peak frequencies, $\theta=30°$, $S_\theta=0$, and water depth $h=6$ m are used. (c) Gaussian directional spectra with varying S_θ, $\theta_m=30°$, and $h=6$ m are used. $S_{xx}/(S_{xx})_{\mathrm{mono}}$ (circle); $S_{yy}/(S_{yy})_{\mathrm{mono}}$ ("x" mark); and $S_{xy}/(S_{xy})_{\mathrm{mono}}$ (square).

Wave Breaking and Roller Model

Surface rollers have an important impact on the surf zone dynamics. For wave-induced longshore currents over barred beaches, it has been shown that including rollers in the wave forcing can give a more accurate longshore velocity profile by shifting the current maximum shoreward and increasing the velocity in the trough areas as well (Reniers and Battjes 1997; Ruessink et al. 2001). The one-dimensional roller energy balance equation has been given by Stive and De Vriend (1994), and Reniers and Battjes (1997), independently. When extended to a 2D time-dependent formulation, the energy balance for rollers can be written as

$$\frac{\partial}{\partial t} E_r + \nabla \cdot [(\mathbf{c}+\mathbf{U})E_r] = -D_r + D_{br} \quad (18)$$

where E_r=roller energy density derived from the kinetic energy density of the roller volume with unit crest length (Svendsen 1984a,b). $\mathbf{c}$ and $\mathbf{U}$=wave phase speed vector and ambient current vector, respectively. The first term on the right-hand side is the roller sink term given by (Duncan 1981; Deigaard 1993)

$$D_r = \frac{E_r g \sin\alpha}{c} \quad (19)$$

where α=wave-front slope and usually is assumed to be $\alpha < 10°$ (Lippmann et al. 1996). D_{br} stands for the wave breaking dissipation and is the source term for the roller energy balance equation.

Using the same strategy as to the wave action balance equation, a roller model including the leading order effects of frequency-and-directional spreading can be derived. While, in the surface roller energy balance equation, the wave phase velocity c is weakly relevant to the frequency σ since surface rollers only exist after wave breaking occurs, therefore, the equation only considering the directional spreading as the following is used:

$$\frac{\partial}{\partial t}E_r + \frac{\partial}{\partial x}\{[c(E_{0,1})_R/E_{0,0} + u]E_r\} + \frac{\partial}{\partial y}\{[c(E_{0,1})_I/E_{0,0} + v]E_r\} = -D_r + D_{br} \quad (20)$$

where $(E_{0,1})_R$ and $(E_{0,1})_I$=real and imaginary parts of the wave moment $E_{0,1}$ as defined previously. However, $(E_{0,1})_R/E_{0,0}$ and $(E_{0,1})_I/E_{0,0}$ contain not only information on the mean wave direction but also the wave directional spreading. Eq. (20) is solved after solving the wave equations with the same numerical schemes. E_r is set to be zero at the offshore boundary.

The formulation of the roller radiation stress is similar to the wave radiation stress. Since c_g=c in shallow water, the roller radiation stress is given by

$$S_{ij,r} = E_r(k_i k_j/k^2 + \delta_{ij}/2) \quad (21)$$

The roller radiation stress is a correction to the wave radiation stress due to the presence of the surface wave rollers. The wave forcing used in later simulations of wave-induced longshore currents includes the effects of the surface wave rollers.

Wave-Driven Longshore Currents

The moments-based reduced spectral wave model of this section is quite well suited to forcing nearshore currents as a coupled wave-circulation system. The circulation model is based on the depth-averaged, nonlinear shallow water equations, which are averaged over the incident wave timescales. This general theoretical treatment is standard in the literature (e.g., Allen et al. 1996) although for the purposes of this paper, we also assume longshore currents to be steady in time (Ruessink et al. 2001)

$$(hu)_x + (hv)_y = 0 \quad (22a)$$

$$(huu)_x + (huv)_y = -gh\eta_x + F_x + \tau_{bx} + \tau'_x \quad (22b)$$

$$(huv)_x + (hvv)_y = -gh\eta_y + F_y + \tau_{by} + \tau'_y \quad (22c)$$

where (u,v)=depth-averaged velocities in the (x,y) directions; h=local water depth; η=mean water surface displacement relative to the undisturbed free surface; g=gravity; τ_{bx} and τ_{by} denote the bottom friction dissipations in the x and y coordinates, respectively. F_x and F_y=wave forcing modeled using the radiation stress concept proposed by Longuet-Higgins and Stewart (1964)

$$F_x = -\frac{1}{\rho}\left(\frac{\partial S_{xx}}{\partial x} + \frac{\partial S_{xy}}{\partial y}\right), \quad F_y = -\frac{1}{\rho}\left(\frac{\partial S_{yx}}{\partial x} + \frac{\partial S_{yy}}{\partial y}\right) \quad (23)$$

where ρ=water density. The radiation stresses are computed from the results of the moments-based approach; thus, the effects of the directional and frequency spreading are included.

The bottom friction (τ_{bx} and τ_{by}) uses the linear damping formulation

$$(\tau_{bx}, \tau_{by}) = c_f U_0(u,v) \quad (24)$$

where U_0=amplitude of the wave horizontal orbital bottom velocity calculated according to the linear wave theory. c_f=empirical drag coefficient. Numerous other formulations have been proposed (e.g., Mei 1983) but, for these purposes, they do not appear to have any clear advantages. A constant c_f with the typical value of O(0.01) from offshore to shoreline has been used by many investigators (e.g., Özkan-Haller and Kirby 1999). A formulation for the variable c_f is proposed by Sleath (1984)

$$c_f = 0.015\left(\frac{k_a}{h}\right)^{1/3} \quad (25)$$

where k_a=apparent bed roughness and is assumed to be constant and time independent. According to Ruessink et al. (2001), k_a is typically in the range of 0.01–0.06 m for simulating longshore currents.

τ'_x and τ'_y represent the effects of the lateral momentum mixing. We use the simple parameterized representation used by Özkan-Haller and Kirby (1999)

$$\tau'_x = 2\frac{\partial}{\partial x}\left(\nu\frac{\partial hu}{\partial x}\right) + \frac{\partial}{\partial y}\left(\nu\frac{\partial hv}{\partial x}\right), \quad \tau'_y = \frac{\partial}{\partial x}\left(\nu\frac{\partial hv}{\partial x}\right) \quad (26)$$

where ν=eddy viscosity coefficient, approximated as $\nu = Mh(\varepsilon_b/\rho)^{1/3}$, where M=a constant mixing coefficient, and ε_b =energy dissipation due to wave breaking. This was developed to parameterize the effects of depth-varying velocities in longshore currents by Putrevu and Svendsen (1999), with typical coefficients of M=0.25 (Özkan-Haller and Kirby 1999). It is worthwhile to note that other processes become important in representations of time-averaged hydrodynamics, namely, the Reynolds stresses arising from lower frequency motions such as shear waves. However, consistent parameterizations of these processes in longshore currents have not been well studied compared to other areas of hydrodynamics. We will instead use the above mixing formulation (26) for both time domain and time-averaged cases, but with larger M values for time-averaged simulations in an attempt to account for these Reynolds stresses.

The numerical circulation model is developed using a pressure-correction solution method (known as the SIMPLE algorithm, which stands for semi-implicit method for pressure-linked equations). It is a finite volume model using structured nonorthogonal computational grids with collocated variable arrangement. The model has second-order accuracy for computational grids.

Simulation of DUCK94 Field Measurement Data

For a first test, we simulate mean alongshore currents driven by wave forcing over a barred beach and compare to the field data. The bathymetry and experimental data used here are from the DUCK94 experiment, which were collected from August to October 1994 during the nearshore field experiments at the U.S. Army Corps of Engineers Field Research Facility (FRF) in Duck, N.C. The wave statistics (the significant wave height H_s, peak period, and mean wave direction) and frequency-directional spectrum were measured at 8-m water depth (Long 1996). Pressure and velocity observations were obtained at more than 15 cross-shore locations extending from the nearshoreline to 4.5-m depth.

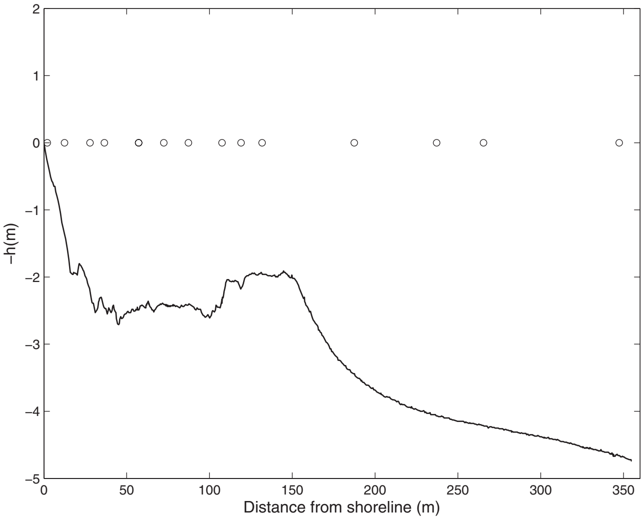

Fig. 6. Sea bottom elevation relative to mean sea level versus cross-shore distance on October 14, 1994 at Duck, N.C. and selected cross-shore locations of pressure sensors and/or current meters

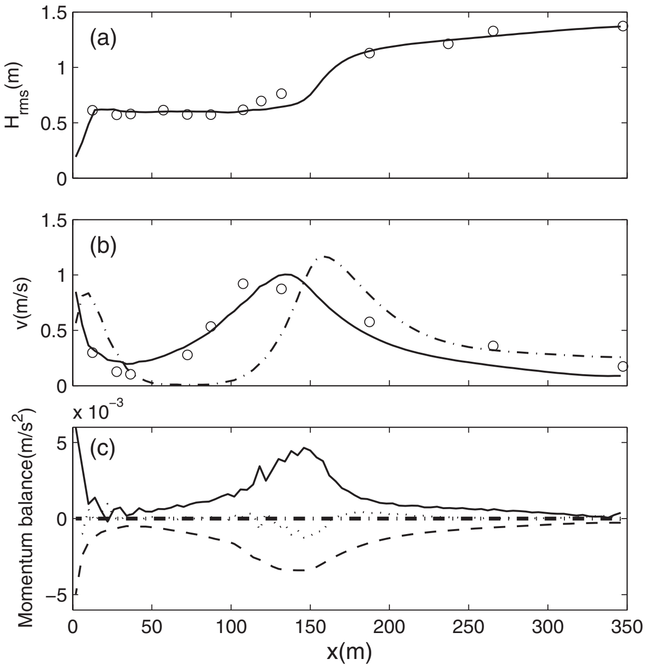

Fig. 7. Model-data comparison: (a) measured (circle) and modeled (solid line) wave height H_{RMS}; (b) longshore current, measured (circle), no roller (dash-dotted line), roller model with $\alpha=0.045$ (solid line); and (c) longshore momentum balance: wave forcing (solid line), bottom friction (long-dashed line), lateral mixing (short-dashed line), and residual (dash-dotted line)

The cross-shore depth profile measured at around 10 a.m. on October 14, 1994 and the locations of the pressure sensors and current meters are shown in Fig. 6. All the wave and current data are 3-h-averaged for a storm event. The 8-m depth wave statistics are $H_s=2.07$ m, $T_p=8.866$ s, and $\theta_m=-20°$. The pressure gauge nearest to the offshore end of the measured bathymetry is P19 located 347.4 m from the shoreline. In order to take advantage of the available wave conditions at Gauge P19, the offshore boundary of the computational domain is chosen to be at the pressure sensor Gauge P19. The wave height and peak period here are $H_{RMS}=1.373$ m and $T_p=6.4$ s.

The bottom morphology for this experiment is known to have been close to alongshore uniform, so alongshore uniformity is also assumed for waves and currents in all numerical experiments. The frequency-directional spectrum at the 8-m water depth is approximated using the Gaussian-shaped spectrum with frequency bandwidth $S_\sigma/\sigma_m=0.14$ and directional bandwidth $S_{\theta 0}=25°$. This specific Gaussian spectrum has the same wave moments $E_{2,0}$ and $E_{0,1}$ as the measured spectrum. The mean wave direction and the frequency and directional bandwidths are transformed to the model offshore boundary (i.e., Gauge P19) using the reduced spectral model assuming a constant slope between the 8-m depth and Gauge P19 as the water depths are not known. The wave field and wave-induced longshore currents from Gauge P19 to the shoreline are simulated using a two-way coupling of the wave and circulation model in which the wave-current interaction is taken into account. The coupling between the models is achieved through radiation stress gradient terms (accounting for the presence of the ambient currents) and through the wave-current interaction terms (leading to the modification of the wave field due to the ambient currents). The simulation results show that the modeled wave height H_{RMS} is in good agreement with the measured data at all sensors [Fig. 7(a)]. The H_{RMS} errors for individual sensors vary between 0.01 and 0.12 m, with an average of 0.04 m for all sensors. The surface rollers were modeled based on Eq. (18) and the wave forcing is calculated including the roller radiation stresses. Fig. 7(b) shows the comparison of predicted longshore currents with/without rollers against the field data. It is clear that by including the roller the predicted longshore velocity profile matches the measurement much better. These simulation results are obtained with $\alpha=0.05$, $k_a=0.017$ m, and $M=1$. The $\alpha=0.05$ and $k_a=0.017$ m are consistent with the values used by Ruessink et al. (2001). It needs to be particularly pointed out that a large lateral mixing coefficient, $M=1$, is used in order to account for the mixing due to the potential instabilities of the mean longshore currents. Ruessink et al. (2001) used a simpler description of lateral mixing in which the eddy viscosity is assumed to be constant. Terms in the y-momentum equation are plotted in Fig. 7(c) with the dash-dotted line representing the residual. The wave forcing is primarily balanced by the bottom friction with the lateral mixing locally important in the surf zone.

Using the same parameters ($\alpha=0.05$, $k_a=0.017$ m, and $M=1$), the influence of the wave frequency and directional spreading was investigated by performing simulations with various nonzero S_σ and S_θ, respectively. The radiation stress component S_{xy} is the most important in simulating alongshore currents because its cross-shore gradient defines the wave forcing and determines the magnitude and cross-shore shape of the resulting longshore currents. As expected, the cross-shore distribution of S_{xy} only varies slightly with increasing the relative frequency bandwidth S_σ/σ_m from 0 to 0.2 for this case [Fig. 8(a)]. As a result, there is no obvious difference in the resulting longshore currents [Fig. 8(b)].

The cross-shore distribution of S_{xy} varying with the directional bandwidth S_θ is shown in Fig. 9(a). S_{xy} displays a nonlinear decrease with increasing S_θ from 0 to 25°. For $S_\theta=5°$ the decrease in S_{xy} is 2%; 8% for $S_\theta=10°$; 16.6% for $S_\theta=15°$; 27% for $S_\theta=20°$; and 38% for $S_\theta=25°$. It appears that the decrease in S_{xy} is initially small and accelerates as the wave directional spreading S_θ increases. The cross-shore shape of S_{xy}, however, does not alter significantly due to the wave directional spreading. The cross-shore profiles of the longshore currents associated with the various S_θ are compared in Fig. 9(b). As expected, the magnitude of

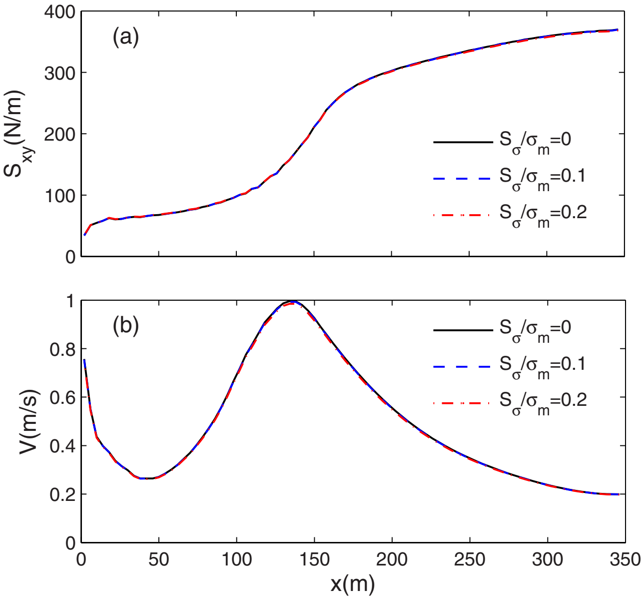

Fig. 8. Effects of frequency spreading on the modeled (a) radiation stress component S_{xy}; (b) longshore current V. $S_\sigma/\sigma_m=0$, no frequency spreading; $S_\sigma/\sigma_m=0.1$ ($S_\sigma=0.098$ rad/s); $S_\sigma/\sigma_m=0.2$ ($S_\sigma=0.196$ rad/s).

the longshore currents is smaller for waves with a broader directional distribution, since S_{xy} is smaller and so is the wave forcing. The shapes of the velocity profiles are similar for all cases with a slight shift of the maximum velocity offshore as S_θ increases. It is also evident that maximum differences in velocity occur in the bar-trough area, with a 35% decrease in $V_{\max}$ as S_θ increases from 0 to 25°. In addition, the jet velocity near the shoreline also decreases substantially as S_θ increases. It should be pointed out that the effect of surface rollers and wave-current interaction were included in all of these simulations.

The bottom friction is a large source of uncertainty because the formulations used are rough approximations and the value of the bottom friction coefficient is not well known a priori. In practice, the friction coefficient is often determined by fitting to observations. As a result, errors in estimated radiation stresses due to

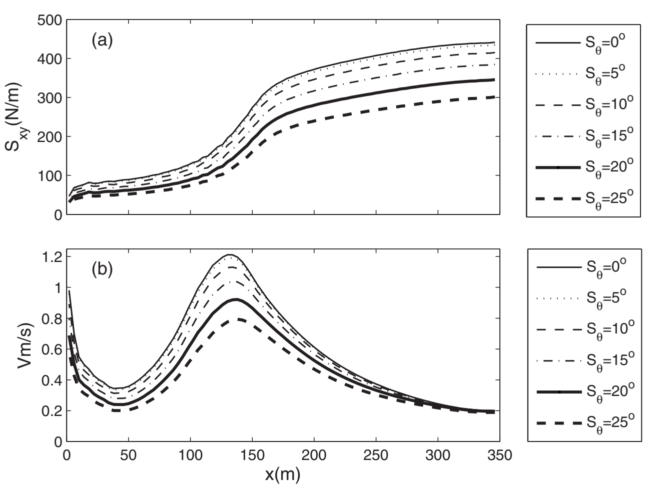

Fig. 9. Effects of directional spreading on the modeled (a) radiation stress component S_{xy}; (b) longshore current V

neglecting the effects of frequency-and-directional spreading will lead to a biased bottom friction coefficient (Battjes 1972; Feddersen 2004). However, it is still unknown how much the presence of the finite frequency and directional spread would alter the resulting mean wave-induced longshore currents, or by matching observations how much the fitted bottom friction coefficient would vary with the frequency and directional spread of the incident waves. In an attempt to address this, the values of the only free parameter in the bottom friction formulation, the bed roughness k_a, associated with various nonzero S_θ were calibrated by matching the observed longshore current velocities as is often done in practice. Strong variations in k_a are observed with increasing S_θ, with k_a decreasing from 0.038 to 0.0072 m as S_θ increases from 0 to 25° (Fig. 10). With k_a=0.038 m, the bottom friction coefficient c_f is in the range of $3.7-4.3\times10^{-3}$ across the bar-trough area, and the cross-shore average c_f is 3.5×10^{-3}. Using k_a=0.0072 m results in the bar-trough c_f ranging from $2.0\sim2.3\times10^{3}$ and the cross-shore average of 2.0×10^{3}. These are significant differences that could lead to errors in longshore currents if the directional bandwidth is neglected.

Discussion and Conclusions

The five-parameter moments-based wave model developed here gives an option intermediate between purely monochromatic-based models and full spectral solutions. Its greatest utility would seem to be in open coast nearshore computations, where the high resolution required to resolve the surf zone is a hindrance for the large-scale application of full spectral models. The improvement in accuracy seems clear over purely monochromatic models and should thus result in an improved prediction of wave-driven longshore currents. Although the results were presented here only for one-dimensional topographies, the numerical extension to two horizontal dimensions has already been implemented and is straightforward. However, this type of model should not be used over strongly varying 2D topographies because of difficulties analogous to the caustics found in monochromatic models.

For single-peaked spectra, probably the most limiting assumption here was the Gaussian closure. Other closures that resemble more closely observed spectra may also be used either with numerical or Taylor series based integrations. However, for nearshore current forcing, the detailed shape of the frequency spectrum has only minor importance. In contrast, the directional distribution is of prime importance and results in strong changes in the modeled currents between narrow and wide directional spreading. The inclusion of directional spreading in the reduced moments model is probably the most important factor to improve the predictions of nearshore currents when compared to monochromatic-based models. Comparisons with measured DUCK94 data showed a strong dependence of the current velocity on the directional bandwidth or, alternatively, in the estimation of the bottom roughness.

Complex multipeaked spectra will not be represented well by this five-moment model. For these spectra that may be found on many coastlines, multiple reduced spectral models with Gaussian closures may be run simultaneously with little additional complexity. An alternative option is the extension to higher-order moments. However, although this is quite possible, closures and integrals and even the choice of moment weighting functions make it a difficult task. This is particularly true for frequency integrals, which are multiplied by group velocities and other frequency-varying functions. Additionally, the simple weighting

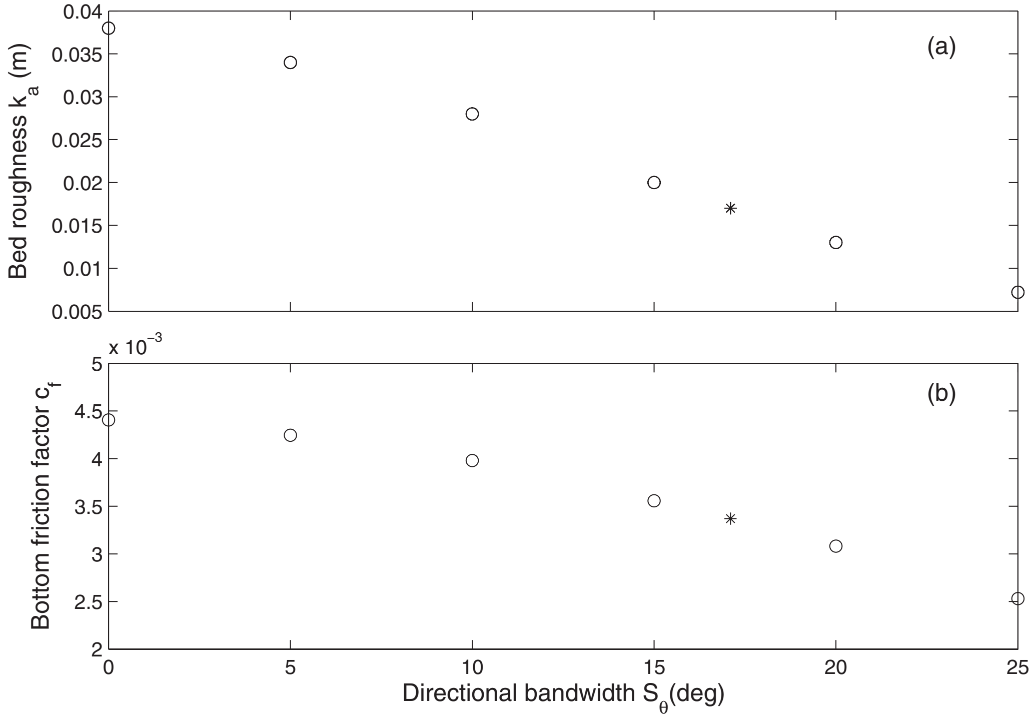

Fig. 10. (a) Variation of apparent bed roughness k_a (m) with directional bandwidth S_θ (deg) obtained by best-fit match to velocity data. (b) Corresponding bottom friction coefficient c_f at the 1.5-m water depth versus directional bandwidth. The asterisk (*) stands for $S_\theta=17.1°$, which is the value of directional bandwidth at the offshore boundary based on the measured wave spectrum at the 8-m water depth.

functions used here will diverge for higher-order frequency moments. An extension to higher-order directional moments may be more accessible, although the development of an arbitrary order directional closure is also an open question. It may prove that, in addition to the five-moment frequency and directionally spread model developed here, an arbitrary order directional model with a constant frequency may be of considerable use in reducing the computational load of full spectral models.

For this simple model to be used mainly for forcing nearshore current models, wind inputs, whitecapping, and nonlinear triad and quadruplet interactions are probably not useful additions. However, if the model were to be extended to higher order for more general use, these would likely increase significantly in importance, and moment-based versions of these sources and sinks would need to be implemented.

Acknowledgments

Funding for this work was provided by the National Science Foundation under Grant No. 0423877 and from Florida Sea Grant under Grant No. R/C-S-46. The DUCK94 current data were downloaded from the U.S. Army Corps of Engineers Field Research Facility and were originally measured by a group including writers of Feddersen et al. (1998).

Appendix I. Derivation of Wave Moments

Derivation of Wave Moments

For the Gaussian-shaped spectra given by Eq. (8), the wave moment $E_{n,m}$ can be written as

$$E_{n,m}=E_{0,0}\frac{1}{\sqrt{2\pi}S_\sigma}\frac{1}{\sqrt{2\pi}S_\theta}\int_0^{+\infty}\sigma^n e^{-1/2[(\sigma-\sigma_m)/S_\sigma]^2}\times d\sigma\int_{-\pi}^{\pi}e^{im\theta}e^{-1/2[(\theta-\theta_m)/S_\sigma]^2}d\theta \quad (27)$$

First, look at the first integral. Let $(\sigma-\sigma_m)/S_\sigma=t$, which gives

$$\int_0^{\infty}\sigma^n e^{-1/2[(\sigma-\sigma_m)/S_\sigma]^2}d\sigma=\int_{-\sigma_m/S_\sigma}^{\infty}(S_\sigma t+\sigma_m)^n e^{-(1/2)t^2}S_\sigma dt \quad (28)$$

Because the exponential function $e^{-(1/2)t^2}$ decreases quickly to 0 as $|t|$ increases to about 3. For relatively narrow spectra, $|-\sigma_m/S_\sigma|$ is always larger than 3. Therefore, it is reasonable to approximate Eq. (28) by

$$\int_0^{\infty}\sigma^n e^{-1/2[(\sigma-\sigma_m)/S_\sigma]^2}d\sigma=\int_{-\sigma_m/S_\sigma}^{\infty}(S_\sigma t+\sigma_m)^n e^{-(1/2)t^2}S_\sigma dt\approx\int_{-\infty}^{\infty}(S_\sigma t+\sigma_m)^n e^{-(1/2)t^2}S_\sigma dt \quad (29)$$

According to the binomial theorem

$$(S_\sigma t+\sigma_m)^n=\sum_{k=0}^{n}\frac{n!}{k!(n-k)!}S_\sigma^{n-k}\sigma_m^k t^{n-k} \quad (30)$$

Substituting Eq. (30) into Eq. (29), it gives

$$\int_0^{\infty}\sigma^n e^{-1/2[(\sigma-\sigma_m)/S_\sigma]^2}d\sigma=\sum_{k=0}^{n}\frac{n!}{k!(n-k)!}S_\sigma^{n-k+1}\sigma_m^k\int_{-\infty}^{+\infty}t^{n-k}e^{-(1/2)t^2}dt$$
$$=\begin{cases}\sum_{k=0}^{n}\frac{n!}{k!(n-k)!}S_\sigma^{n-k+1}\sigma_m^k 2^{(n-k+1)/2}\Gamma[(n-k+1)/2], & (n-k)=0,2,4,\ldots\\ 0, & \text{otherwise}\end{cases}\tag{31}$$

where $\Gamma[(n-k+1)/2]$=gamma function.

Similar processes are applied to the integral $\int_{-\pi}^{\pi}e^{-1/2[(\theta-\theta_m)/S_\sigma]^2}d\theta$. Substituting $\theta-\theta_m/S_\theta=t$ into the integral and assuming that both $|(\pi-\theta_m)/S_\theta|$ and $|(-\pi-\theta_m)/S_\theta|$ are not small so that the approximation followed can be made

$$\int_{-\pi}^{\pi}e^{im\theta}e^{-1/2[(\theta-\theta_m)/S_\theta]^2}d\theta=\int_{(-\pi-\theta_m)/S_\theta}^{(\pi-\theta_m)/S_\theta}e^{im(S_\theta t+\theta_m)}e^{-(1/2)t^2}S_\theta dt\approx\sqrt{2\pi}S_\theta e^{-m^2S_\theta^2/2}e^{im\theta_m}\tag{32}$$

Combining Eqs. (31) and (32), the moment $E_{n,m}$ is finally given by

$$E_{n,m}=\frac{E_{0,0}}{\sqrt{2\pi}}e^{-m^2S_\theta^2/2}e^{im\theta_m}\begin{cases}\sum_{k=0}^{n}\frac{n!}{k!(n-k)!}S_\sigma^{n-k+1}\sigma_m^k 2^{(n-k+1)/2}\Gamma\left(\frac{(n-k+1)}{2}\right), & (n-k)=0,2,4,\ldots\\ 0, & \text{otherwise}\end{cases}\tag{33}$$

As mentioned above, $|\sigma_m/S_\sigma|$, $|(\pi-\theta_m)/S_\theta|$, and $|(-\pi-\theta_m)/S_\theta|$ were assumed to be no less than 3 in order to take advantage of the definite integral containing exponential functions. To maintain the assumption valid, the following limitations are forced:

$$S_\sigma/\sigma_m\leqslant 0.25,\ (\pi-\theta_m)/S_\theta\geqslant 5 \text{ and } (-\pi-\theta_m)/S_\theta\leqslant -5\tag{34}$$

After deriving the general form of the wave moment $E_{n,m}$, it is straightforward to give the moments appearing in the current wave model

$$E_{0,1}=E_{0,0}\sigma_m,\quad E_{0,2}=E_{0,0}(\sigma_m^2+S_\sigma^2),\quad E_{0,m}=E_{0,0}e^{-m^2S_\theta^2/2}e^{im\theta_m}\tag{35}$$

Evaluation of the Integrals in Wave Governing Equations

The propagation velocities in σ-space can be rewritten as

$$c_\sigma=\frac{1}{h}(\mathbf{U}\cdot\nabla h)\left(\frac{c_g}{c}-\frac{1}{2}\right)\sigma-\frac{c_g}{c}\sigma\left[\cos^2\theta\frac{\partial u}{\partial x}+\sin\theta\cos\theta\left(\frac{\partial u}{\partial y}+\frac{\partial v}{\partial x}\right)+\sin^2\theta\frac{\partial v}{\partial y}\right]\tag{36}$$

$$c_\theta=-\frac{1}{h}\left(c_g-\frac{1}{2}c\right)\left(-\sin\theta\frac{\partial h}{\partial x}+\cos\theta\frac{\partial h}{\partial y}\right)-\left[\cos^2\theta\frac{\partial u}{\partial y}-\sin\theta\cos\theta\left(\frac{\partial u}{\partial x}-\frac{\partial v}{\partial y}\right)-\sin^2\theta\frac{\partial v}{\partial x}\right]\tag{37}$$

First Integral

$$\begin{aligned}I1&=\int_0^{\infty}\int_{-\pi}^{\pi}(\mathbf{c_g}+\mathbf{u})\sigma^n e^{im\theta}Fd\sigma d\theta\\&=\int_0^{\infty}\int_{-\pi}^{\pi}\left(\frac{e^{i\theta}+e^{-i\theta}}{2},\frac{e^{i\theta}-e^{-i\theta}}{2i}\right)c_g\sigma^n e^{im\theta}E_{0,0}M(\sigma)D(\theta)d\sigma d\theta\\&+(u,v)E_{n,m}=\frac{1}{2}[E_{0,m+1}+E_{0,m-1},-i(E_{0,m+1}-E_{0,m-1})]\\&\times\int_0^{\infty}c_g\sigma^n M(\sigma)d\sigma+(u,v)E_{n,m}\end{aligned}\tag{38}$$

Using the Taylor expansion of c_g, we have

$$\begin{aligned}I1&=\frac{1}{2}A_1[E_{n,m+1}+E_{n,m-1},-i(E_{n,m+1}-E_{n,m-1})]\\&+\frac{1}{2}A_2[E_{n+1,m+1}+E_{n+1,m-1},-i(E_{n+1,m+1}-E_{n+1,m-1})]\\&+\frac{1}{2}A_3[E_{n+2,m+1}+E_{n+2,m-1},-i(E_{n+2,m+1}-E_{n+2,m-1})]\\&+(u,v)E_{n,m}\end{aligned}\tag{39}$$

where

$$A_1=(c_g)_{\sigma_m}-\sigma_m\left(\frac{\partial c_g}{\partial\sigma}\right)_{\sigma_m}+\frac{1}{2}\sigma_m^2\left(\frac{\partial^2 c_g}{\partial\sigma^2}\right)_{\sigma_m}$$
$$A_2=\left(\frac{\partial c_g}{\partial\sigma}\right)_{\sigma_m}-\sigma_m\left(\frac{\partial^2 c_g}{\partial\sigma^2}\right)_{\sigma_m},\quad A_3=\frac{1}{2}\left(\frac{\partial^2 c_g}{\partial\sigma^2}\right)_{\sigma_m}$$

Second Integral

Similar to the first integral, the second integral can be given by

$$I2=\int_0^{+\infty}\int_{-\pi}^{\pi} c_\theta \sigma^n e^{im\theta} F d\sigma d\theta$$

$$=-\frac{1}{2h}A_4\left[i\frac{\partial h}{\partial x}(E_{n,m+1}-E_{n,m-1})+\frac{\partial h}{\partial y}(E_{n,m+1}+E_{n,m-1})\right]$$
$$-\frac{1}{2h}A_5\left[i\frac{\partial h}{\partial x}(E_{n+1,m+1}-E_{n+1,m-1})+\frac{\partial h}{\partial y}(E_{n+1,m+1}+E_{n,m-1})\right]$$
$$-\frac{1}{2h}A_6\left[i\frac{\partial h}{\partial x}(E_{n+2,m+1}-E_{n+2,m-1})+\frac{\partial h}{\partial y}(E_{n+2,m+1}+E_{n+2,m-1})\right]$$
$$-\frac{1}{4}\frac{\partial u}{\partial y}(2E_{n,m}+E_{n,m+2}+E_{n,m-2})-\frac{i}{4}\left(\frac{\partial u}{\partial x}-\frac{\partial v}{\partial y}\right)$$
$$\times(E_{n,m+2}-E_{n,m-2})+\frac{1}{4}\frac{\partial v}{\partial x}(2E_{n,m}-E_{n,m+2}-E_{n,m-2}) \quad (40)$$

where

$$A_4=(c_g-c/2)_{\sigma_m}-\sigma_m\left[\frac{\partial}{\partial\sigma}(c_g-c/2)\right]_{\sigma_m}+\frac{1}{2}\sigma_m^2\left[\frac{\partial^2}{\partial\sigma^2}(c_g-c/2)\right]_{\sigma_m}$$

$$A_5=\left[\frac{\partial}{\partial\sigma}(c_g-c/2)\right]_{\sigma_m}-\sigma_m\left[\frac{\partial^2}{\partial\sigma^2}(c_g-c/2)\right]_{\sigma_m}$$

$$A_6=\frac{1}{2}\left[\frac{\partial^2}{\partial\sigma^2}(c_g-c/2)\right]_{\sigma_m}$$

Third Integral

$$I3=\int_0^{+\infty}\int_{-\pi}^{\pi} c_\sigma \sigma^{n-1} e^{im\theta} F d\sigma d\theta$$

$$=\frac{1}{h}(\mathbf{U}\cdot\nabla h)\left[\left(A_7-\frac{1}{2}\right)E_{n,m}+A_8E_{n+1,m}+A_9E_{n+2,m}\right]$$
$$-\frac{1}{4}A_7\left[\frac{\partial u}{\partial x}(2E_{n,m}+E_{n,m+2}+E_{n,m-2})-i\left(\frac{\partial u}{\partial y}+\frac{\partial v}{\partial x}\right)\right.$$
$$\left.\times(E_{n,m+2}-E_{n,m-2})+\frac{\partial v}{\partial y}(2E_{n,m}-E_{n,m+2}-E_{n,m-2})\right]$$
$$-\frac{1}{4}A_8\left[\frac{\partial u}{\partial x}(2E_{n+1,m}+E_{n+1,m+2}+E_{n+1,m-2})-i\left(\frac{\partial u}{\partial y}+\frac{\partial v}{\partial x}\right)\right.$$
$$\left.\times(E_{n+1,m+2}-E_{n+1,m-2})+\frac{\partial v}{\partial y}(2E_{n+1,m}-E_{n+1,m+2}-E_{n+1,m-2})\right]$$
$$-\frac{1}{4}A_9\left[\frac{\partial u}{\partial x}(2E_{n+2,m}+E_{n+2,m+2}+E_{n+2,m-2})-i\left(\frac{\partial u}{\partial y}+\frac{\partial v}{\partial x}\right)\right.$$
$$\left.\times(E_{n+2,m+2}-E_{n+2,m-2})+\frac{\partial v}{\partial y}(2E_{n+2,m}-E_{n+2,m+2}-E_{n+2,m-2})\right] \quad (41)$$

where

$$A_7=\left(\frac{c_g}{c}\right)_{\sigma_m}-\sigma_m\left(\frac{\partial}{\partial\sigma}\frac{c_g}{c}\right)_{\sigma_m}+\frac{1}{2}\sigma_m^2\left(\frac{\partial^2}{\partial\sigma^2}\frac{c_g}{c}\right)_{\sigma_m},\quad A_8=\left(\frac{\partial}{\partial\sigma}\frac{c_g}{c}\right)_{\sigma_m}-\sigma_m\left(\frac{\partial^2}{\partial\sigma^2}\frac{c_g}{c}\right)_{\sigma_m},\quad A_9=\frac{1}{2}\left(\frac{\partial^2}{\partial\sigma^2}\frac{c_g}{c}\right)_{\sigma_m}.$$

Explicit Equations for Regular Directional Waves

For waves with one single frequency (i.e., $S_\sigma=0$) and Gaussian direction distribution, and no ambient currents, the governing equations can be written in explicit form as follows:

$$\frac{\partial}{\partial t}E_{0,0}+\nabla\cdot[E_{0,0}c_ge^{-S_\theta^2/2}(\cos\theta_m,\sin\theta_m)]=0 \quad (42)$$

$$\frac{\partial}{\partial t}E_{0,1}+\frac{1}{2}\frac{\partial}{\partial x}[E_{0,0}c_g(e^{-2S_\theta^2}e^{2i\theta_m}+1)]+\frac{1}{2}\frac{\partial}{\partial y}[-iE_{0,0}c_g(e^{-2S_\theta^2}e^{2i\theta_m}-1)]+\frac{1}{2h}E_{0,0}\left(c_g-\frac{1}{2}c\right)\times\left[-\frac{\partial h}{\partial x}(e^{-2S_\theta^2}e^{2i\theta_m}-1)+i\frac{\partial h}{\partial y}(e^{-2S_\theta^2}e^{2i\theta_m}+1)\right]=0 \quad (43)$$

Appendix II. Spectral Wave Breaking Model

For irregular waves, the spectral and directional details of depth-induced wave breaking are not well understood and little is known about how to simulate numerically. Fortunately, the total energy dissipation due to depth-induced breaking has been studied and can be well modeled based on different theories such as the bore-based breaking model (Battjes and Janseen 1978) and the random wave transformation model by Thornton and Guza (1983). Laboratory observations indicate that the shape of a wave spectrum changes only moderately as waves propagate cross a simple beach profile. Based on this, Eldeberky and Battjes (1996) developed a spectral version of the breaking model of Battjes and Janseen (1978)

$$S_{br}(\sigma,\theta)=\frac{D_{\rm tot}}{E_{\rm tot}}F(\sigma,\theta) \quad (44)$$

where S_{br}=source term due to the wave breaking; $D_{\rm tot}$=rate of total energy dissipation due to the wave breaking; and $E_{\rm tot}$=total wave energy equivalent to $E_{0,0}$ defined in the wave model.

Lim and Chan (2003) incorporated different breaking models into the SWAN wave model and evaluated their performance by comparing with experimental data and concluded that the model of Thornton and Guza (1983) yielded the smallest errors. In the present model, the breaking model of Thornton and Guza will be incorporated and the slightly modified version by Whitford (1988) based on a best fit to the field data is used

$$D_{\rm tot}=\frac{3\sqrt{\pi}}{16}f_pB^3C_1\frac{H_{\rm RMS}^3}{h}\left\{1-\left[1+\left(\frac{H_{\rm RMS}}{\gamma h}\right)^2\right]^{-2.5}\right\} \quad (45)$$

where

$$C_1=1+\tanh\left[8\left(\frac{H_{\rm RMS}}{\gamma h}-0.99\right)\right] \quad (46)$$

in which f_p=peak frequency; the coefficient B=0.8 (measuring the intensity of the wave breaking); and γ=0.42.

To develop a wave breaking model fit to the current wave model, similar operations apply to the breaking dissipation term $S_{br}(\sigma,\theta)$. Multiplying Eq. (44) by $\sigma^n e^{im\theta}$ and integrating over the frequencies and directions, we can have

$$\int_0^{+\infty}\int_{-\pi}^{\pi}\sigma^n e^{im\theta}S_{br}d\sigma d\theta = \int_0^{+\infty}\int_{-\pi}^{\pi}\frac{D_{\text{tot}}}{E_{0,0}}\sigma^n e^{im\theta}Fd\sigma d\theta = \frac{D_{\text{tot}}}{E_{0,0}}E_{n,m} \tag{47}$$

in which the RMS wave height in D_{tot} can be evaluated by $E_{0,0}$ with the following relation: $H_{\text{RMS}}=\sqrt{8E_{0,0}}$.

According to Eq. (47), the breaking dissipation terms associated with the equations of moments $E_{0,0}$, $E_{1,0}$, $E_{2,0}$, and $E_{0,1}$ are the following, respectively:

$$\int_0^{+\infty}\int_{-\pi}^{\pi}S_{br}d\sigma d\theta = D_{\text{tot}} \tag{48}$$

$$\int_0^{+\infty}\int_{-\pi}^{\pi}\sigma S_{br}d\sigma d\theta = D_{\text{tot}}\sigma_m \tag{49}$$

$$\int_0^{+\infty}\int_{-\pi}^{\pi}(\sigma-\sigma_m)^2 S_{br}d\sigma d\theta = D_{\text{tot}}S_\sigma^2 \tag{50}$$

$$\int_0^{+\infty}\int_{-\pi}^{\pi}e^{i\theta}S_{br}d\sigma d\theta = D_{\text{tot}}\frac{E_{01}}{E_{00}} \tag{51}$$

Thus, the dissipation due to breaking is included in this wave model by including the breaking terms given by Eqs. (47)–(51). The energy dissipation rate D_{tot} is infinitesimally small when no breaking happens but increases to finite values after the waves start breaking. It may be worth mentioning that no assumption has been made in developing this breaking model. Therefore, this breaking model itself is not limited to narrowbanded regular spectra.

References

Allen, J. S., Newberger, P. A., and Holman, R. A. (1996). "Nonlinear shear instabilities of alongshore currents on plane beaches." *J. Fluid Mech.*, 310, 181–213.

Battjes, J. A. (1972). "Radiation stresses in short-crested waves." *J. Mar. Res.*, 30, 56–64.

Battjes, J. A., and Janseen, J. P. F. M. (1978). "Energy loss and setup due to breaking of random waves." *Proc., 16th Int. Conf. Coastal Engineering*, ASCE, New York, 569–587.

Booij, N., Ris, R. C., and Holthuijsen, L. H. (1999). "A third-generation wave model for coastal regions. Part I: Model description and validation." *J. Geophys. Res.*, 104(C4), 7649–7666.

Bowen, A. J. (1969). "Rip currents: 1. Theoretical investigations." *J. Geophys. Res.*, 74, 5467–5478.

Chawla, A., Özkan, H. T., and Kirby, J. T. (1998). "Spectral model for wave transformation and breaking over irregular bathymetry." *J. Waterway, Port, Coastal, Ocean Eng.*, 124(4), 189–198.

Chen, Q., Kirby, J. T., Dalrymple, R. A., Shi, F., and Thornton, E. B. (2003). "Boussinesq modeling of longshore currents." *J. Geophys. Res.*, 108(C11), 3362–3379.

Church, J. C., and Thornton, E. B. (1993). "Effects of breaking wave induced turbulence within a longshore current model." *Coastal Eng.*, 20, 1–28.

Deigaard, R. (1993). "A note on the three dimensional shear stress distribution in a surfzone." *Coastal Eng.*, 20, 157–171.

Duncan, J. H. (1981). "An experimental investigation of breaking waves produced by a towed hydrofoil." *Proc. R. Soc. London, Ser. A*, 377, 331–348.

Eldeberky, Y., and Battjes, J. A. (1996). "Spectral modeling of wave breaking: Application to Boussinesq equations." *J. Geophys. Res.*, 101(C1), 1253–1264.

Elgar, S., Herbers, T. H. C., and Guza, R. T. (1994). "Reflection of ocean surface gravity waves from a natural beach." *J. Phys. Oceanogr.*, 24, 1503–1511.

Feddersen, F. (2004). "Effect of wave directional spread on the radiation stress: Comparing theory and observations." *Coastal Eng.*, 51, 473–481.

Feddersen, F., Guza, R. T., Elgar, S., and Herbers, T. H. C. (1998). "Alongshore momentum balances in the nearshore." *J. Geophys. Res.*, 103, 15667–15676.

Guza, R. T., Thornton, E. B., and Christensen, N. (1986). "Observations of steady longshore currents in the surf zone." *J. Phys. Oceanogr.*, 16, 1959–1969.

Hasselmann, K., Barnett, T. P., Bouws, E., Carlson, H., Cartwright, D. E., Enke, K., Ewing, J. A., Gienapp, H., Hasselmann, D. E., Kruseman, P., Meerburg, A., Müller, P., Olbers, D. J., Richter, K., Sell, W., and Walden, H. (1973). "Measurements of wind-wave growth and swell decay during the Joint North Sea Wave Project (JONSWAP)." *Dtsch. Hydrogr. Z.*, 12, 1–95.

Holthuijsen, L. H. (1983). "Observations of the directional distribution of ocean-wave energy in fetch-limited conditions." *J. Phys. Oceanogr.*, 13, 191–207.

Holthuijsen, L. H. (2007). *Waves in oceanic and coastal waters*, Cambridge University Press, New York.

Kuik, A. J., van Vledder, G. Ph., and Holthuijsen, L. J. (1988). "A method for the routine analysis of pitch-and-roll wave buoy data." *J. Phys. Oceanogr.*, 18, 1020–1034.

Lim, S. H. L., and Chan, E. S. (2003). "Surf zone wave modeling—Improvement of dissipation by depth-induced wave breaking in SWAN." *Proc., 10th OMISAR Workshop on Ocean Models*, APEC/MRC/OMISAR, Hanoi, Vietnam.

Lippmann, T. C., Brookins, A. H., and Thornton, E. B. (1996). "Wave energy transformation on natural profiles." *Coastal Eng.*, 27, 1–20.

Long, C. E. (1996). "Index and bulk parameters for frequency-direction spectra measured at CERC Field Research Facility, June 1994 to August 1995." *Misc. Pap. No. CERC-96-6*, U.S. Army Engineering Waterway Experiment Station, Vicksburg, Miss.

Longuet-Higgins, M. S. (1970). "Longshore currents generated by obliquely incident sea waves. I.." *J. Geophys. Res.*, 75, 6778–6789.

Longuet-Higgins, M. S., and Stewart, R. W. (1964). "Radiation stresses in water waves: A physical discussion with applications." *Deep-Sea Res.*, 11, 529–562.

Mei, C. C. (1983). "The applied dynamics of ocean surface waves." *Advanced series on coastal engineering*, Vol. 1, World Scientific, Singapore.

Özkan-Haller, H. T., and Kirby, J. T. (1999). "Nonlinear evolution of shear instabilities of the longshore current: A comparison of observations and computations." *J. Geophys. Res.*, 104(C11), 25953–25984.

Panchang, V. G., Wei, G., Pearce, B. R., and Briggs, M. J. (1990). "Numerical simulation of irregular wave propagation over shoal." *J. Waterway, Port, Coastal, Ocean Eng.*, 116(3), 324–340.

Pierson, W. J., and Moskowitz, L. (1964). "A proposed spectral form for fully developed wind seas based on the similarity theory of S. A. Kitaigorodskii." *J. Geophys. Res.*, 69, 5181–5190.

Putrevu, U., and Svendsen, I. A. (1999). "Three-dimensional dispersion of momentum in wave-induced nearshore currents." *Eur. J. Mech. B/Fluids*, 18, 409–427.

Reniers, A. J. H. M., and Battjes, J. A. (1997). "A laboratory study of longshore currents over barred and non-barred beaches." *Coastal Eng.*, 30, 1–21.

Ruessink, B. G., Miles, J. R., Feddersen, F., Guza, R. T., and Elgar, S. (2001). "Modeling the alongshore current on barred beaches." *J. Geophys. Res.*, 106, 22451–22463.

Sleath, J. F. A. (1984). *Sea bed mechanics*, Wiley, New York.

Stive, M. J. F., and De Vriend, H. J. (1994). "Shear stress and mean flow in shoaling and breaking waves." *Proc., 24th Int. Coastal Engineering Conf.*, ASCE, New York, 594–608.

Svendsen, I. A. (1984a). "Wave heights and setup in a surf zone." *Coastal Eng.*, 8, 303–329.

Svendsen, I. A. (1984b). "Mass flux and undertow in a surf zone." *Coastal Eng.*, 8, 347–365.

Thornton, E. B. (1970). "Variation of longshore current across the surf zone." *Proc., 12th Coastal Engineering Conf.*, ASCE, New York, 291–308.

Thornton, E. B., and Guza, R. T. (1983). "Transformations of wave height distribution." *J. Geophys. Res.*, 88, 5925–5938.

Thornton, E. B., and Guza, R. T. (1986). "Surf zone longshore currents and random waves: Field data and models." *J. Phys. Oceanogr.*, 16(7), 1165–1178.

Tolman, H. L. (1991). "A third-generation model for wind waves on slowly varying, unsteady and inhomogeneous depths and currents." *J. Phys. Oceanogr.*, 21(6), 782–797.

Vincent, C. L., and Briggs, M. J. (1989). "Refraction-diffraction of irregular waves over a mound." *J. Waterway, Port, Coastal, Ocean Eng.*, 115(2), 269–284.

WAMDI Group. (1988). "The WAM model—A third generation ocean wave prediction model." *J. Phys. Oceanogr.*, 18, 1775–1810.

Whitford, D. J. (1988). "Wind and wave forcing of longshore currents across a barred beach." Ph.D. dissertation, Nav. Postgrad. School, Monterey, Calif.

Willebrand, J. (1975). "Energy transport in a nonlinear and inhomogeneous random gravity wave field." *J. Fluid Mech.*, 70, 113–126.